Lawrence Berkeley National Laboratory
Recent Work

Title

Initial Characterization of a Position-Sensitive Photodiode/BGO Detector for PET

Permalink

https://escholarship.org/uc/item/3nf172xm

Journal

IEEE Transactions on nuclear science, 36(1)

Authors

Derenzo, S.E.
Moses, W.W.
Jackson, H.G.
et al.

Publication Date

2017-12-04

Lawrence Berkeley Laboratory

UNIVERSITY OF CALIFORNIA

Initial Characterization of a Position-Sensitive Photodiode/BGO Detector for PET

S.E. Derenzo, W.W. Moses, H.G. Jackson, B.T. Turko, J.L. Cahoon, A.B. Geyer, and T. Vuletich

November 1988

Donne

Biology &
Medicine
Division

DISCLAIMER

Initial Characterization of a Position-Sensitive Photodiode/BGO Detector for PET

S.E. Derenzo, W.W. Moses, H.G. Jackson, B.T. Turko,
J.L. Cahoon, A.B. Geyer, and T. Vuletich

Research Medicine and Radiation Biophysics Division
Lawrence Berkeley Laboratory
1 Cyclotron Road
Berkeley, California 94720

November 1988

INITIAL CHARACTERIZATION OF A POSITION-SENSITIVE PHOTODIODE/BGO DETECTOR FOR PET

S.E. Derenzo, W.W. Moses, H.G. Jackson,
B.T. Turko, J.L. Cahoon, A.B. Geyer, and T. Vuletich,
Donner Laboratory and Lawrence Berkeley Laboratory,
University of California, Berkeley, CA 94720

Abstract

We present initial results of a position-sensitive photodiode/BGO detector for high resolution, multi-layer positron emission tomography (PET). Position sensitivity is achieved by dividing the 3 mm x 20 mm rectangular photosensitive area along the diagonal to form two triangular segments. Each segment was individually connected to a low-noise charge amplifier. The photodiodes and crystals were cooled to -100 °C to reduce dark current and increase the BGO signal. With an amplifier peaking time of 17 μsec, the sum of the signals (511 keV photopeak) was 3200 electrons with a full width at half maximum (fwhm) of 750 electrons. The ratio of one signal to the sum determined the depth of interaction with a resolution of 11 mm fwhm.

1 Introduction

This paper describes a new position sensitive photodiode and its ability to measure the depth of interaction of 511 keV annihilation photons in narrow BGO crystals. It includes considerations of light collection, diode design, and contributions to electronic noise. It also shows the design for a multi-layer high resolution positron tomograph using this detector element.

In previous work we showed that if two 3 mm wide BGO crystals are coupled to the same phototube, then individually coupled, cooled, low-noise silicon photodiodes can determine the crystal of interaction with high reliability [1]. While HgI_2 [2]–[5] and silicon avalanche diodes [6] have advantages as photodetectors in this application, they are not yet commercially available at a reasonable cost.

In contrast, most positron tomographs use small BGO or BaF_2 crystals, and couple each crystal to several larger phototubes using a variety of coding schemes that permit the relative phototube pulse height to be used to determine the crystal of interaction [7]–[15]. While these designs minimize the number of phototubes and provide multi-layer PET, the low light output of BGO and BaF_2 results in statistical fluctuations in the position measurements, which appears to limit the in-plane spatial resolution to about 4.5 mm fwhm.

Individual crystal/phototube readout overcomes this limitation, as demonstrated by the small animal system built in Chiba, Japan [16], and the Donner 600-crystal tomograph [17]. We propose the use of individually coupled photodiodes to preserve this spatial resolution while reducing the number of phototubes

A serious problem remaining, especially for the highest resolution positron tomographs, is the radial blurring resulting from crystal penetration for sources away from the axis of the system. As an example of the effect of penetration, at the center of the field the Donner 600-crystal tomograph has a circular point spread function with 2.6 mm fwhm, but at 8 cm from the center the point spread function is elliptical with 2.7 mm x 4.2 mm fwhm [17]. Solutions to this problem involve mathematical restoration of the tomograph data [18] or measuring the depth of interaction in the detector. Two NaI(Tl)-based tomographs use the high light output of this scintillator to measure the width of the light distribution and infer the depth of interaction [19], [20]. Other designs use staggered layers of BGO, GSO and BaF_2 coupled to phototubes [21], or layers of tilted BGO and GSO scintillators coupled to silicon avalanche photodiodes [6]. In these, the observed decay time is used to determine the crystal of interaction. Other approaches use a three dimensional array of many small plastic scintillators coupled to phototubes by many long lightpipes [22], or position-sensitive mesh-dynode phototubes coupled to a bundle of long, thin BGO crystals [23]. We propose to solve the radial blurring problem by measuring the depth of interaction with the same position sensitive photodiode that performs the crystal identification.

2 Crystal/Photodiode Detector Module

The detectors used in this work consisted of a 3 mm x 10 mm x 25 mm deep BGO crystal, with a specially fabricated position-sensitive silicon photodiode coupled to a 3 mm x 25 mm crystal face. (The crystals were manufactured by Harshaw Chemical Co., Solon, Ohio, and the photodiodes were manufactured by Micron Semiconductor, Ltd., England.) The photodiodes were divided into two triangular segments (Fig. 1) and each segment was connected to separate charge amplifiers and filter circuits, with outputs A and B. The sum A+B represents the energy deposited in the crystal and the ratio A/(A+B) is a measure of the center of intensity of the photons along the length of the photodiode.
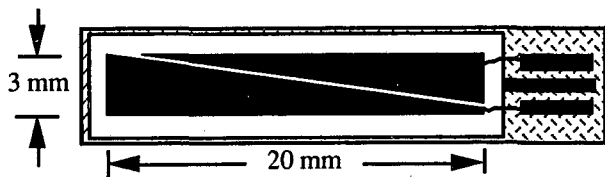
Fig. 1. Position-sensitive silicon photodiode. Each triangular segment is connected to a charge amplifier

2.1 Light Collection

When a 511 keV annihilation photon interacts in the BGO crystal, scintillation photons are emitted isotropically along the short (<1 mm) track of the recoil electron. Some of these photons are reflected by the interior crystal surfaces or scatter on the external reflector before entering the photodiode and contribute to a spatially diffuse component. Other photons take a more direct path and enter the photodiode after travelling a short distance. This direct component is spread in the 3 mm dimension but retains some localization along the 25 mm direction. In section 3 we estimate the fraction of photons in each component.

2.2 Charge Amplifiers

Each photodiode was provided with two charge amplifiers. The first stage of the charge amplifier (Fig. 2), implemented with surface mount components, was mounted 6 mm from the photodiode, and was at the same temperature as the BGO crystal and photodiode. The cascode amplifier and filter stage was on a printed circuit board about 25 cm away, and at room temperature. When the entire charge amplifier is at room temperature, the amplifier noise (fwhm electrons) for pure capacitive loads is given by

$$N_{fwhm} = 365 + 5.7 \, C$$

where C is the capacitance in pF. The addition of a series resistor greatly increases the noise. For example, a 10 kΩ series resistance (typical for a 3 x 20 mm p-layer) doubles the noise of a 30 pF load. It is therefore important that the photodiode have low series resistance.
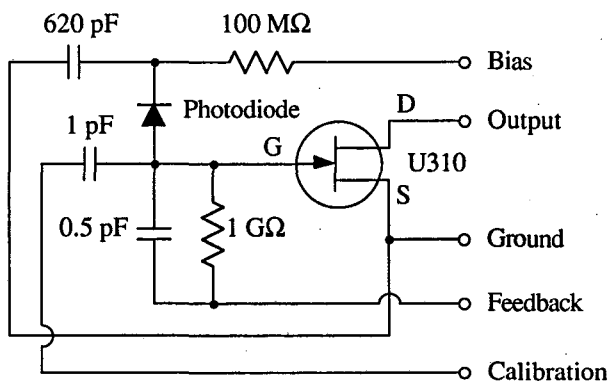

Fig. 2. Photodiode and first stage of charge amplifier

2.3 Photodiode Properties

The capacitance of the photodiode and the associated amplifier noise is decreased with increasing reverse bias, until it reaches an asymptotic level [24]. However, this reverse bias introduces dark current and an associated shot noise, which are reduced by cooling. Table I lists the dark current and expected shot noise for several temperatures between +20°C and –60°C. The shot noise (in electrons fwhm) was estimated from reference [25] for RC-CR pulse shaping:

$$N_{fwhm} = 2.35 \sqrt{12 \, I_d \, T}$$ (1)

where T is the amplifier peaking time in nsec, and I_d is the dark current in nA.

TABLE I[a]

Temperature (°C)	Dark current (nA)[b]	Shot noise (fwhm e⁻)[c]
20	20	4700
0	3	1800
–20	0.2	470
–40	0.015	130
–60	0.001	30

[a] 50 V reverse bias, amplifier peaking time 17 μsec
[b] Typical – actual values may vary by a factor of 2
[c] From equation 1

Measurements on initial photodiode samples showed electronic noise that was significantly above that of a capacitor of equivalent value. This was attributed to series resistance in the optically transparent p-layer and was eliminated in the diodes used in this work by the addition of a grid of fine aluminum strips incorporated into the p-layer.

Table II lists the capacitance and electronic noise level for diodes of three thicknesses equipped with aluminum grids at a 50 V reverse bias and –100 °C. The noise level of 900 electrons fwhm at a thickness of 307 μm is unusually high and is attributed to a problem in fabrication. While the 596 μm diode has the lowest capacitance, it may not be fully depleted and its noise may be higher due to series resistance in the n-type layer.

TABLE II[a]

Diode thickness (μm)	Capacitance[b] (pF)	Noise (fwhm e⁻)
307	17.5	900
506	16.5	510
596	13	600

[a] –100°C, 50 V reverse bias, amplifier peaking time 17 μsec
[b] per triangular segment

Early tests also showed that wire bonds connecting the photodiode p-layer and n-layer contacts to the solder pads on the ceramic base were not able to withstand repeated temperature cycling between room temperature and –100°C. The breakage occurred at the solder pads and was eliminated by bonding the wire to small solid gold pins that had been pressed into holes into the ceramic.

3   Results

3.1   Set-Up

A beam of 511 keV annihilation photons was defined by a 3 mm wide BGO crystals mounted on a phototube and a positron source as shown in Fig. 3. A second 3 mm wide BGO crystal was coupled to a phototube and a position-sensitive photodiode. A metal screen at ground potential was placed between the phototube and the latter crystal to shield the photodiode and charge amplifiers from electronic pulses within the phototube. The charge amplifier sum A+B and the ratio A/(A+B) was recorded for each phototube-phototube coincidence as the positron annihilation beam was swept along the length of the crystal and photodiode.

3.2   Pulse height

Fig. 4 shows the distribution of the sum A+B for 511 keV incident photons. It is clear that the silicon photodiode can distinguish between noise and photopeak pulses with high reliability. The ability to identify individual crystals makes possible the use of this detector design for multi-layer, high-resolution PET.
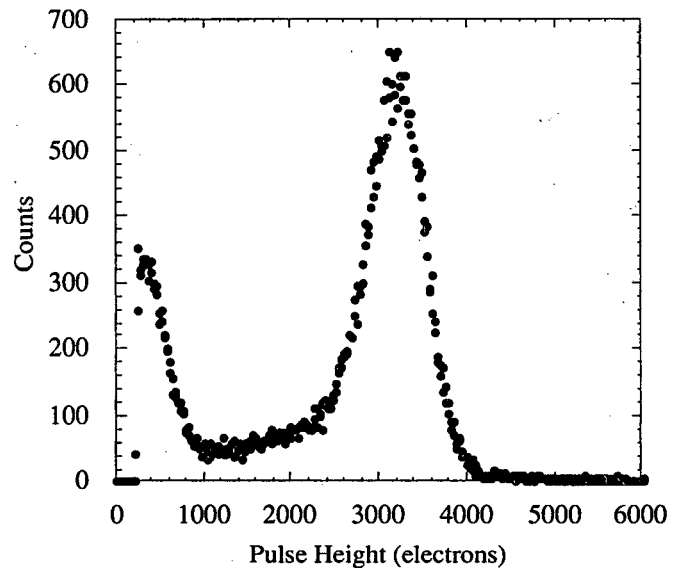
Fig. 4 Pulse height distribution of BGO/photodiode signal A+B for 511 keV annihilation photons at –100°C using a peaking time of 17 μsec.

3.3   Position sensitivity

When the annihilation photon beam was swept along the length of the BGO crystal and photodiode, the amplifier sum A+B showed little variation from x = 0 mm (the front of the crystal) to x = 15 mm, and dropped by about 23% at x = 25 mm (the extreme end of the crystal) because at that point the crystal extended beyond the photodiode (top curve, Fig. 5). The ratio η = A/(A+B) dropped steadily from 0.72 at 2.5 mm to 0.45 at 15 mm (bottom curve, Fig. 5) and has an average slope $d\eta/dx$ = 0.020 mm^{-1}. A straight line through this part of the curve is given by equation 2.
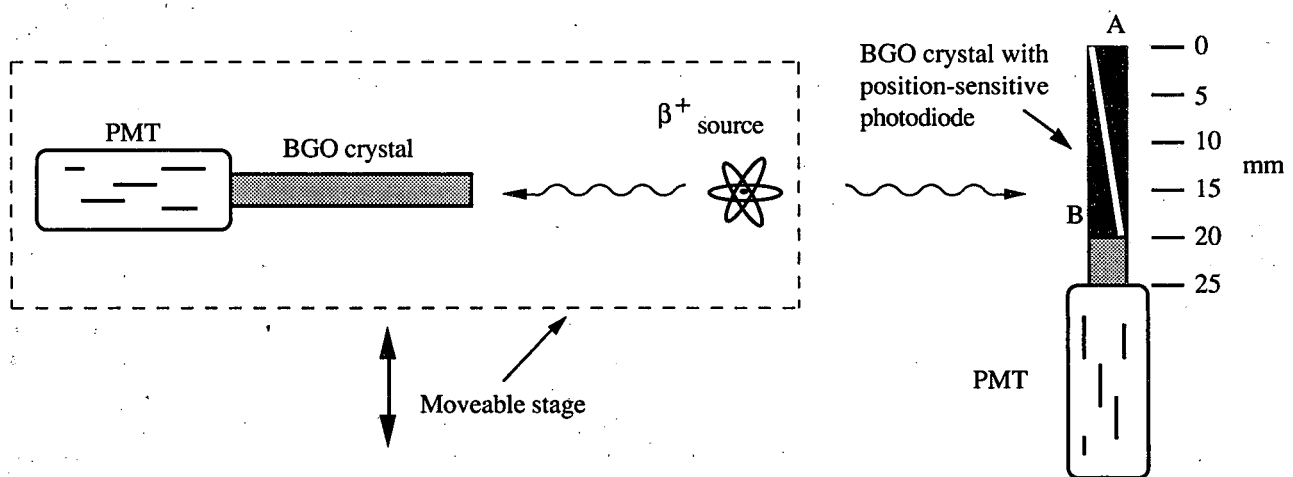
Fig. 3. Experimental set-up for measuring the position sensitivity of the BGO/photodiode detector. The annihilation photon beam is defined by a coincidence between the two phototubes. The silicon photodiode, BGO crystal, and PMT assembly (right side Fig. 3) were cooled to –100°C.

$$\eta = 0.76 - 0.020\, x. \qquad (2)$$

The weak dependence of η on x near x = 0 mm is expected due to total internal reflection at the end surface of the crystal. The smaller slope beyond 17.5 mm is due to the limited length of the photodiode and the loss of the direct component. At x = 25 mm, both A and B are due to diffuse components only, and we expect A/(A+B) = 0.50, as observed.

We derive an expression for the ideal relationship between A/(A+B) and the position x, assuming that the photodiode covers the entire length L of the crystal and a certain position independent fraction f of the detected light is diffuse and the remaining fraction d is direct. We have:

$$A = 0.5f + (1 - x/L)d,$$

$$B = 0.5f + xd/L$$

$$\eta = \frac{A}{A+B} = \frac{0.5f + (1 - x/L)d}{f+d}$$

$$\text{at } x = 0, \quad \eta = 1 - \frac{0.5f}{f+d} \qquad (3)$$

$$\text{at } x = L, \quad \eta = \frac{0.5f}{f+d}$$

$$\frac{d\eta}{dx} = \frac{-d/L}{f+d} \qquad (4)$$

Relating the measured intercept of equation (2) with equation (3), we have d/(f+d) = 0.52 and f/(f+d) = 0.48. Relating the measured slope of equation (2) with equation (4) for L = 20 mm, we have d/(f+d) = 0.40 and f/(f+d) = 0.60. We conclude that about 54% of the light detected by the photodiode is diffuse and 46% is direct.

In a separate experiment, the diffuse white external reflector on the BGO crystal was replaced with an aluminized mylar specular reflector in an attempt to increase the fraction of direct light. This treatment did not help, and the measured values of A/(A+B) vs position were nearly identical in both cases.

The error bars shown in the lower curve of Fig. 5 are the fwhm of the distribution of η, not the uncertainty in the average value of η. The average η(fwhm) is 0.216. Propagating this to the fwhm in position x, we have:

$$x(\text{ fwhm }) = \frac{\eta(\text{fwhm})}{d\eta/dx} = \frac{0.216}{0.020} = 10.8 \text{ mm}$$

Fig. 6 shows the distribution of η for x = 0 mm and x = 15 mm. The peaks are well separated, and it appears possible to determine whether the interaction occurred in the front, middle, or rear portions of a 25 mm deep crystal with a fair degree of reliability.
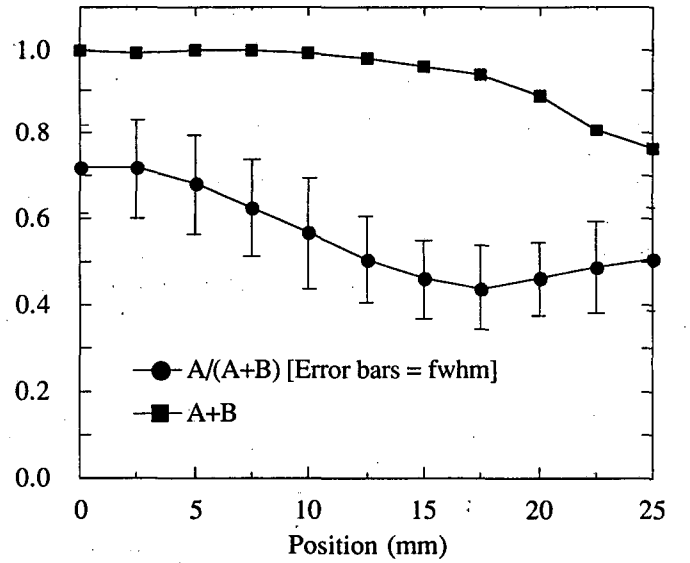

Fig. 5   Relative pulse height of the 511 keV photopeak (A+B) and the ratio A/(A+B) as a function of beam position. The set-up and beam coordinate system are shown in Fig. 3.
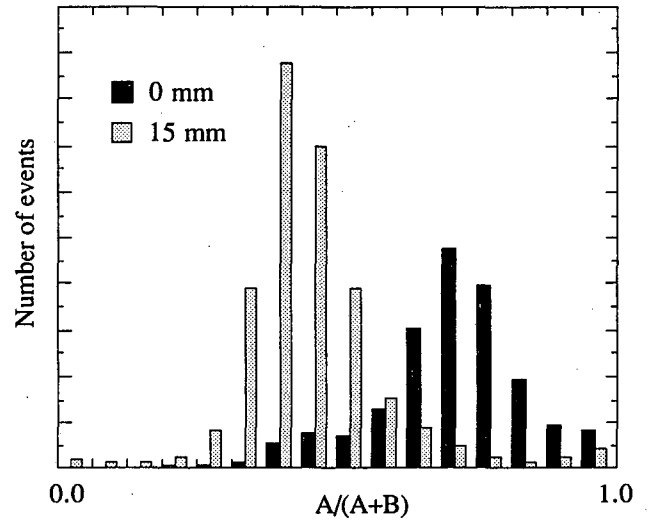

Fig. 6. Plot of A/(A+B) for beam positions 0 and 15 mm. The set-up and beam coordinate system are shown in Fig. 3.

4   Future Developments

We are continuing the development of improved position-sensitive photodiodes, with the goal of measuring the depth of interaction with a resolution < 5 mm fwhm, using peaking times < 5 μsec. In addition to the photodiode described in this paper, we are also interested in the Gatti/Rehak silicon drift photodiode, which has very low noise due to its low capacitance (< 1 pF), and the ability to sense position by measuring the drift time of the charge carriers [26], [27].

Our goal is the development of a multi-slice positron tomograph with over 10,000 crystals and a 2 mm in-plane spatial resolution over the entire imaging field. For this application, we propose a detector consisting of three or more optically isolated BGO crystals attached to a single 10 mm square photomultiplier tube, which provides a fast timing pulse for the group (Fig. 7). Each crystal is also individually coupled to a position-sensitive photodiode that identifies the crystal that stopped the annihilation photon and determines the depth of interaction. We are developing low-cost surface-mount charge amplifiers that can be used to read out thousands of cooled position-sensitive photodiodes.
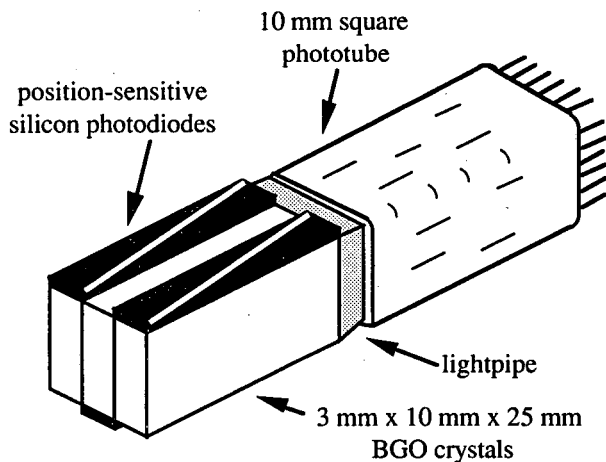

Fig. 7. Detector assembly of three BGO crystals, three position-sensitive photodiodes, and a square phototube.

5 Conclusions

1. The BGO/silicon photodiode detector provides a signal of 3200 electrons with a fwhm of 750 electrons and an amplifier noise of 650 electrons fwhm. This permits crystal identification with high reliability.

2. The position-sensitive silicon photodiode can measure the depth of interaction with an accuracy of about 11 mm fwhm.

3. About 46% of the photodiode signal is due to the direct photon component that provides the depth information. The remaining 54% is due to the diffuse component.

4. The best signal to noise is not necessarily achieved with the thickest photodiode. Very thick diodes may have series resistance due to the incomplete depletion.

5. Reduction of noise due to series resistance requires a grid of conductive aluminum on the P-layer.

6. Temperature cycling can cause separation of the wire bond from the ceramic substrate. This problem is solved by bonding to gold pins pressed into holes in the ceramic.

References

[1] S. E. Derenzo, "Initial characterization of a BGO-silicon photodiode detector for high resolution PET," *IEEE Trans Nucl Sci*, vol. NS-31, pp. 620-626, 1984.

[2] J. B. Barton, E. J. Hoffman, J. S. Iwanczyk, et al., "A high-resolution detection system for positron tomography," *IEEE Trans Nucl Sci*, vol. NS-30, pp. 671-675, 1983.

[3] J. S. Iwanczyk, J. B. Barton, A. J. Dabrowski, et al., "A novel radiation detector consisting of an HgI2 photodetector coupled to a scintillator," *IEEE Trans Nucl Sci*, vol. NS-30, pp. 363-367, 1983.

[4] M. Dahlbom, M. A. Mandelkern, E. J. Hoffman, et al., "Hybrid mercuric iodide (HgI2) -- gadolinium orthosilicate (GSO) detector for PET," *IEEE Trans Nucl Sci*, vol. NS-32, pp. 533-537, 1985.

[5] J. M. Markakis, "Mercuric iodide photodetector-cesium iodide scintillator gamma ray spectrometers," *IEEE Trans Nucl Sci*, vol. NS-35, pp. 356-359, 1988.

[6] C. Carrier, C. Martel, D. Schmitt, et al., "Design of a high resolution positron emission tomograph using solid state scintillation detectors," *IEEE Trans Nucl Sci*, vol. NS-35, pp. 685-690, 1988.

[7] K. Takami, K. Ishimatsu, T. Hayashi, et al., "Design considerations for a continuously rotating positron computed tomograph," *IEEE Trans Nucl Sci*, vol. NS-29, pp. 534-538, 1982.

[8] A. Ricci, E. Hoffman, M. Phelps, et al., "Investigation of a technique for providing a pseudo-continuous detector ring for positron tomography," *IEEE Trans Nucl Sci*, vol. NS-29, pp. 452-456, 1982.

[9] C. A. Burnham, D. E. Kaufman, D. A. Chesler, et al., "Cylindrical PET detector design," *IEEE Trans Nucl Sci,* vol. NS-35, pp. 675-679, 1988.

[10] J. M. Roney and C. J. Thompson, "Detector identification with 4 BGO crystals on a dual PMT," *IEEE Trans Nucl Sci,* vol. NS-31, pp. 1022-1027, 1984.

[11] M. E. Casey and R. Nutt, "A multicrystal two dimensional BGO detector system for positron emission tomography," *IEEE Trans Nucl Sci,* vol. NS-33, pp. 460-463, 1986.

[12] S. Yamamoto, S. Miura and I. Kanno, "A BGO detector using a new encoding scheme for a high resolution positron emission tomograph," *Nucl Instr Meth,* vol. A248, pp. 557-561, 1986.

[13] S. Holte, L. Eriksson, J. E. Larsson, et al., "A preliminary evaluation of a positron camera system using weighted decoding of individual crystals," *IEEE Trans Nucl Sci,* vol. NS-35, pp. 730-734, 1988.

[14] H. B. Min, J. B. Ra, K. J. Jung, et al., "Detector identification in a 4x4 BGO crystal array coupled to two dual PMTs for high resolution positron emission tomography," *IEEE Trans Nucl Sci,* vol. NS-34, pp. 332-336, 1987.

[15] W. H. Wong, M. Jing, B. Bendriem, et al., "A slanting light-guide analog decoding high resolution detector for positron emission tomography camera," *IEEE Trans Nucl Sci,* vol. NS-34, pp. 280-284, 1987.

[16] T. Tomitani, N. Nohara, H. Murayama, et al., "Development of a high resolution positron CT for animal studies," *IEEE Trans Nucl Sci,* vol. NS-32, pp. 822-825, 1985.

[17] S. E. Derenzo, R. H. Huesman, J. L. Cahoon, et al., "A positron tomograph with 600 BGO crystals and 2.6 mm resolution," *IEEE Trans Nucl Sci,* vol. NS-35, pp. 659-664, 1988.

[18] R. H. Huesman, E. M. Saleron and J. R. Baker, "Compensation for crystal penetration in high resolution positron emission tomography," *IEEE Trans Nucl Sci,* vol. NS-36, 1989 (submitted).

[19] J. S. Karp and M. E. Daube-Witherspoon, "Determination of depth-of-interaction in scintillation crystals using a temperature gradient," *Nucl Instr Meth,* vol. A260, pp. 509-517, 1987.

[20] J. G. Rogers, R. Harrop, P. E. Kinahan, et al., "Conceptual design of a whole body PET machine," *IEEE Trans Nucl Sci,* vol. NS-35, pp. 680-684, 1988.

[21] W. H. Wong, "Designing a stratified detection system for PET cameras," *IEEE Trans Nucl Sci,* vol. NS-33, pp. 591-596, 1986.

[22] J. A. McIntyre, R. L. Spross and K. H. Wang, "Construction of a positron emission tomograph with 2.4 mm detectors," *IEEE Trans Nucl Sci,* vol. NS-33, pp. 425-427, 1986.

[23] K. Shimizu, T. Ohmura, M. Watanabe, et al., "Development of 3-D detector system for positron CT," *IEEE Trans Nucl Sci,* vol. NS-35, pp. 717-720, 1988.

[24] S. E. Derenzo, "Gamma-ray spectroscopy using small, cooled bismuth germanate scintillators and silicon photodiodes," *Nucl Instr Meth,* vol. 219, pp. 117-122, 1984.

[25] H. G. Spieler and E. E. Haller, "Assessment of present and future large-scale semiconductor detector systems," *IEEE Trans Nucl Sci,* vol. NS-32, pp. 419-426, 1985.

[26] E. Gatti and P. Rehak, "Semiconductor drift chamber- an application of a novel charge transport scheme," *Nucl Instr Meth,* vol. A225, pp. 608-614, 1984.

[27] L. Strüder, G. Lutz, M. Sterzik, et al., "First tests with fully depleted PN-CCD's," *IEEE Trans Nucl Sci,* vol. NS-35, pp. 372-376, 1988.

LAWRENCE BERKELEY LABORATORY
TECHNICAL INFORMATION DEPARTMENT
1 CYCLOTRON ROAD
BERKELEY, CALIFORNIA 94720